Crustal thermal regime prior to, during and following rifting: A geochronological and modelling study of the Mesozoic South-Alpine rifted margin.

Bertotti, G.V.; Wijbrans, J.R.; Seward, D.; ter Voorde, M.; Hurford, T.

published in
Tectonics
1999

DOI (link to publisher)
10.1029/1998TC900028

document version
Publisher's PDF, also known as Version of record

TECTONICS, VOL. 18, NO. 2, PAGES 185-200, APRIL 1999

Crustal thermal regime prior to, during, and after rifting: A geochronological and modeling study of the Mesozoic South Alpine rifted margin

G. Bertotti,[1] D. Seward,[2] J. Wijbrans,[1] M. ter Voorde,[1] and A. J. Hurford [3]

Abstract. An approximately 15-km-thick segment of the Mesozoic passive continental margin of Adria was involved in Alpine shortening and is now exposed in the Lake Como-Lake Lugano area (southern Alps, northern Italy and southern Switzerland). The segment comprises the Monte Generoso basin, a deep (~9 km) extensional basin controlled by the activity of the Lugano-Val Grande normal fault. The paleosurface and Mesozoic geometric relations are well preserved so that the kinematics of fault blocks prior to, during, and after extension are well constrained. Rb/Sr, $^{40}Ar/^{39}Ar$ and zircon fission track data from basement rocks underlying at various the Generoso basin depths, provide independent estimates on the thermal evolution of the crustal segment during and after rifting. Most Rb/Sr and $^{40}Ar/^{39}Ar$ ages are contemporaneous with the initial stages of rifting (Late Triassic to Early Jurassic) documenting (1) strongly altered thermal conditions before the onset of extension and (2) cooling throughout rifting. Thermal gradients decreased from >60°C km^{-1} at the onset of extension to ~20°C km^{-1} shortly after breakup. Zircon fission track ages are Jurassic to Early Cretaceous providing evidence for continued cooling until the beginning of Alpine shortening. Thermokinematic numerical modeling of the considered crustal segment provides a full, two-dimensional description of synrift and postrift evolution. Synthetic time versus temperature curves are extracted from the model and compared with those derived from absolute ages.

1. Introduction

The thermal evolution of a crustal segment undergoing rifting is the net result of various, often competing, kinematic and thermal processes which must be quantitatively assessed in order to obtain reliable reconstructions and predictions. Mass movements occurring during rifting are related to normal faulting and isostatic compensation of loads. Thermal changes can be attributed to (1) lithospheric thinning, (2) fault-controlled mass movements, and (3) possible emplacement of magmatic bodies. One method to determine the thermal evolution of basement rocks is through absolute age dating. In general, however, interpretation of these data has proven difficult because of the intrinsic difficulty of translating closing/annealing temperatures into depths in the absence of an independently determined geothermal gradient (especially in periods of tectonic activity when this is expected to change) [*Lister and Baldwin,* 1993]. Crustal-scale numerical models have been derived in the last years which have improved our knowledge of the thermal and mechanic evolution of rifted margins [e.g., *Buck,* 1991; *Govers and Wortel,* 1993; *Bassi,* 1995]. Well-constrained case studies are, however, uncommon mainly because of the difficulty of obtaining relevant data from the deep part of margins which have not been involved in subsequent orogenies.

The Late Jurassic to Cretaceous Southern Alps formed a segment of the passive margin of the Adriatic plate (Figures 1 and 2) [*Bernoulli et al.,* 1979; *Bertotti et al.,* 1993a]. A section of the upper 15 km of this margin is now exposed in the Lake Como-Lake Lugano area (Southern Alps, northern Italy) (Figures 2 and 3) and was affected by tectonic and thermal processes taking place during the formation of the South Alpine rifted margin: it was heated during a Middle Triassic thermal event and was stretched and thinned during Late Triassic to Middle Jurassic rifting. Subsequently, the section remained tectonically inactive until the Late Cretaceous when it was involved in Alpine shortening, undergoing, however, limited internal disruption. Prerift, synrift and postrift mass movements are fairly well known in the Lake Lugano-Lake Como region both from the sedimentary record [*Bernoulli,* 1964] and from structural investigations [*Bertotti,* 1991; *Bertotti et al.,* 1993b]. The area represents therefore, an ideal locality to study the thermal processes related to the various stages of rifting.

Unlike the western Southern Alps, where a wealth of absolute age determinations exists [e.g., *Hunziker et al.,* 1992], only few isotopic data have been published from the central South Alpine area [*Mottana et al.,* 1985; *Sanders et al.,* 1996]. We have determined new ages using Rb/Sr, $^{40}Ar/^{39}Ar$, and fission track (FT) techniques on various minerals in the Lake Como region. These are the first $^{40}Ar/^{39}Ar$ spectra and fission track data published. Integrating these data with the independently derived kinematic evolution of the crustal sector considered, we describe the Mesozoic thermal evolution of the South Alpine crust prior to, during, and after rifting. We then present the results of thermal-kinematic numerical modeling and compare synthetic time versus temperature curves derived for various points of the South Alpine crust with absolute ages obtained from corresponding samples.

The proposed reconstruction has important implications for the understanding of the thermal evolution of continental rifts associated with passive margin formation. Despite a long-

[1] Faculty of Earth Sciences, Vrije Universiteit, Amsterdam
[2] Geologisches Institut Eidgenossische Technische Hochschule, Zurich
[3] University College London, London

Paper number 1998TC900028.
0278-7407/99/1998TC900028$12.00

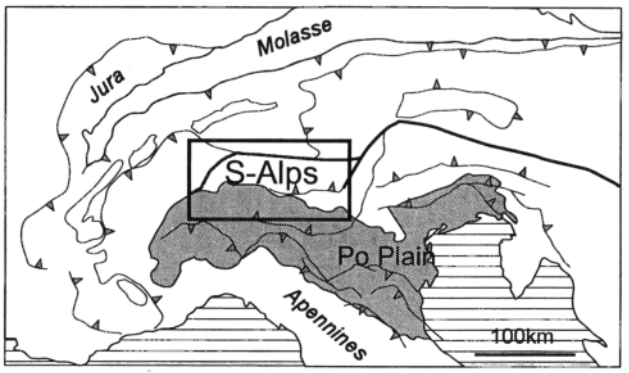

Figure 1. Generalized map of the Alps. The outlined rectangle indicates the position of the western Southern Alps and corresponds to the map of Figure 2a.

standing debate, relationships between continental rifting and thermal evolution, especially in the initial stages, remain poorly documented and disputed [e.g. *Olsen and Morgan,* 1995]. In this paper we also aim at providing greatly needed quantitative estimates for rates of first-order geological processes such as movements of fault blocks and of isotherms during and after tectonically active periods.

2. The Tectonic Framework

In the Southern Alps (Figure 1), Upper Permian to Lower Triassic clastics deposited in a partly continental setting stratigraphically overlie the deeply eroded Variscan basement [*Assereto et al.,* 1973]. During the Middle Triassic marine transgression a system of carbonate platforms and intervening basins developed. Thickness variations occur, but they are of regional extent and do not seem to be fault controlled [*Brack and Rieber,* 1993, and references therein]. Various lines of evidence, such as volcanic rocks below the Po Plain [e.g. *Brusca et al.,* 1981], pegmatites emplaced at middle crustal levels [*Sanders et al.,* 1996], Sensitive High Resolution Microprobe (SHRIMP) data on zircons [*Vavra et al.,* 1996], and numerical modeling [*Bertotti and ter Voorde,* 1994] suggest strongly anomalous thermal conditions associated with significant Middle Triassic magmatism [*Ferrara and Innocenti,* 1974; *Mottana et al.,* 1985]. Geological evidence, such as the presence of volcanic erosional products in Carnian sandstones [*Garzanti,* 1985], as well as conventional K-Ar [*Mottana et al.,* 1985] and new Rb-Sr data [*Sanders et al.,* 1996] suggest that the heat source was deactivated in the Carnian and that cooling took place from the Late Triassic onward. Continental rifting affected the central and western Southern Alps beginning in the Norian (~223 Ma according to the timescale of *Odin* [1994] which we will follow) [*Bertotti et al.,* 1993a] (Figure 3). Until the Late Liassic (~186 Ma), extension was localized in the central Southern Alps and caused the formation of the Lombardian basin (Figure 2) which was controlled in the west by the east dipping Lago Maggiore and Lugano-Val Grande faults and in the east by the west dipping Sebino and Garda faults. In the Late Liassic, extension gradually shifted to the west of the Lombardian basin, west of the Canavese region where breakup eventually occurred in the Middle Jurassic [*Ohnenstetter et al.,* 1981; *Bill et al.,* 1997]. The passive margin stage, during which only little sediment accumulated [*Bernoulli,* 1964; *Winterer and Bosellini,* 1981], continued until the Late Cretaceous when Alpine contraction began [e.g., *Schmid et al.,* 1997].

The area of the current study is the Lake Lugano-Lake Como region (Figures 2a and 3a). It is traversed by the Lugano-Val Grande normal fault which has long been recognized as a Mesozoic normal fault [*Vonderschmitt,* 1940; *Bernoulli,* 1964] and is, in fact, one of the major faults associated with the formation of the South Alpine rifted margin [*Bernoulli et al.,* 1979; *Bertotti,* 1991] (Figures 2c and 3a). The

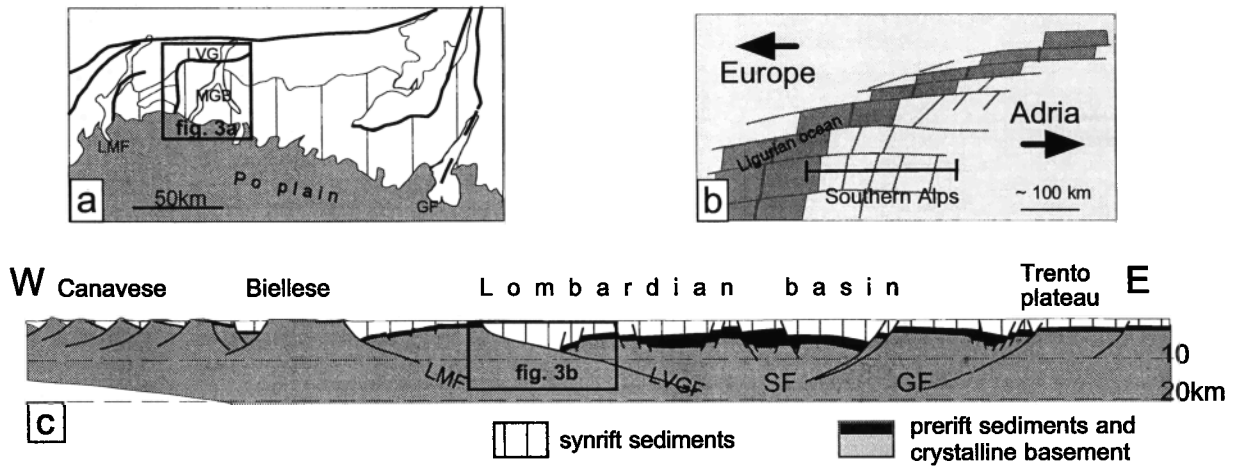

Figure 2. (a) Present-day setting of the Southern Alps. The outlined square shows the Lake Como-Lake Lugano area at the center of this study (Figure 3a). (b) Plate tectonic configuration in the Late Jurassic. The solid line on the Adriatic plate shows the South Alpine section of the Adriatic margin and roughly corresponds to the trace of the profile of Figure 2c. (c) Late Jurassic profile across the passive margin of Adria. The outlined rectangle indicates the position of the Monte Generoso basin and crustal section and corresponds to the profile shown in Figure 3b. Abbreviations are as follows: LMF, Lago Maggiore fault; LVGF, Lugano-Val Grande fault; SF, Sebino fault; GF, Garda fault; MGB, Monte Generoso basin.

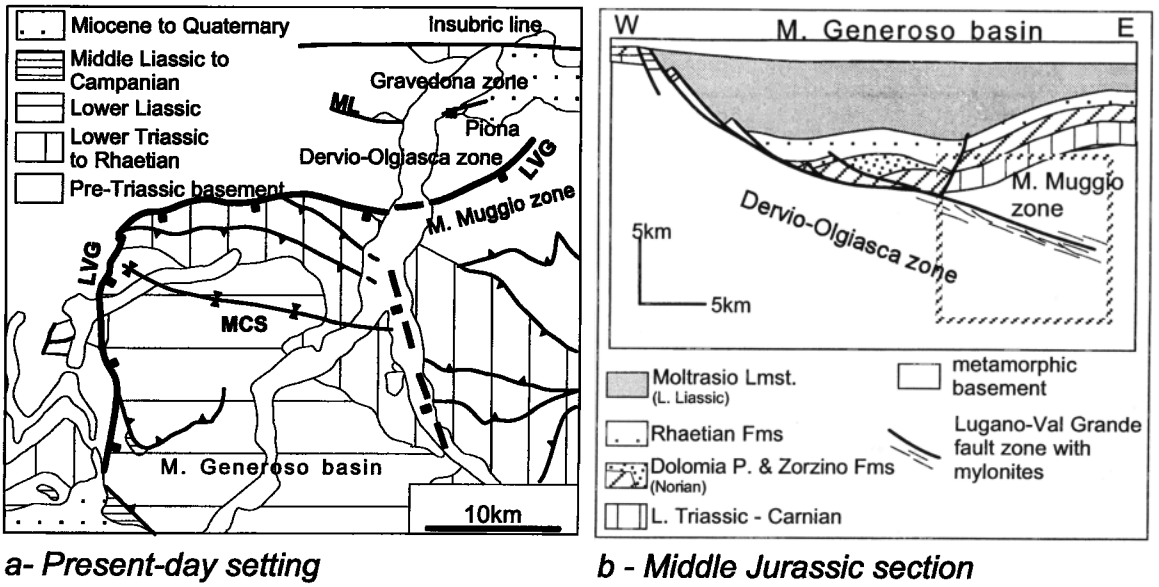

Figure 3. (a) Schematic geologic map of the Monte Generoso basin and surrounding areas (position given in Figure 2a). Abbreviations are as follows: LVG, Lugano-Val Grande fault; MCS, Monte Cecci syncline; and ML, Musso Line. (b) Middle Jurassic profile through the Monte Generoso basin and underlying crust. The position of the section is shown in Figure 2c. The outlined square shows the Jurassic position of the upper Lake Como transect. Reprinted from *Bertotti et al.* [1993b], copyright 1991, with permission from Elsevier Science.

Lugano-Val Grande fault controlled the opening of the Monte Generoso basin, one of the largest sedimentary basins of the margin [*Bernoulli,* 1964].

The present-day regional geology (Figure 3a) is characterized by Variscan basement rocks to the west and north of the Lugano-Val Grande fault and Upper Permian to Liassic sediments east and south of it. Sediments increase in age from south to north. West of Lake Como, the contact between sediments and basement occurs along the Lugano-Val Grande fault and is therefore tectonic. East of Lake Como, the Lugano-Val Grande fault is intracrystalline and separates two basement units: the Monte Muggio zone with its Upper Permian to Lower Triassic sedimentary cover in the south and the Dervio-Olgiasca zone in the north (Figure 3a) [*El Tahlawi,* 1965; *Diella et al.,* 1992]. The Dervio-Olgiasca zone is limited to the north by the Musso Line. The Lugano-Val Grande fault zone, as exposed along Lake Como, is formed by a several hundred meters thick, steeply south dipping band of fault rocks ranging from greenschist mylonites in the north to cataclasites in the south [*Bertotti,* 1991; *Bertotti et al.,* 1993b].

The overall structure of the area is interpreted in terms of a two-stage evolution [*Bally et al.,* 1981; *Bertotti,* 1991]: (1) Late Triassic to Liassic extension along the N-S trending, east dipping Lugano-Val Grande normal fault (a hanging wall and a footwall are thus defined to the east and to the west, respectively, of the Lugano-Val Grande fault) and (2) roughly N-S Alpine contraction during which a WNW-ESE trending syncline developed (Monte Cecci syncline [*Bernoulli,* 1964]) and steepened Paleozoic to Mesozoic rocks and structures in the northern part of the area (Figure 3a). For all practical purposes, the present-day map view of the region south of the Musso Line can be considered as a partially disturbed Mesozoic vertical profile with deeper Mesozoic levels being exposed from south to north.

From this scheme, rocks south and east of the Lugano-Val Grande fault are part of the hanging wall, while rocks to the west and north belong to the footwall. Removing the Alpine deformation, a section through the Monte Generoso basin at the end of extension (Middle Jurassic) can be constructed (Figure 3b). The Lugano-Val Grande fault presumably had a listric shape and acted as a discrete fault/shear zone from the surface down to a depth of at least 15 km (Figure 2). A vertical displacement of 8-10 km has been estimated on the base of the different sediment thicknesses of the footwall and hanging wall [*Bertotti,* 1991].

3. Geochronology

3.1. Rb/Sr

Samples were collected along a N-S profile along the eastern side of Lake Como. The results from the Mesozoic deepest position (Piona) have been published by *Sanders et al.* [1996]; we integrate here that section with samples from the Dervio-Olgiasca zone (Figure 4). Unfortunately, rocks from the Monte Muggio zone were highly weathered and proved unsuitable for Rb/Sr dating. Pegmatite ages were calculated on the basis of the K-feldspar-muscovite couple, while muscovite-biotite was used for the schists, and calcite-white mica was used for the marble (Table 1).

The ages (Figure 4 and Table 1) fall between 215 and 195 Ma. We could detect no clear younging trend in N-S direction, suggesting rapid cooling (< few million years) of the crustal section. In the Piona samples, pegmatites show older ages

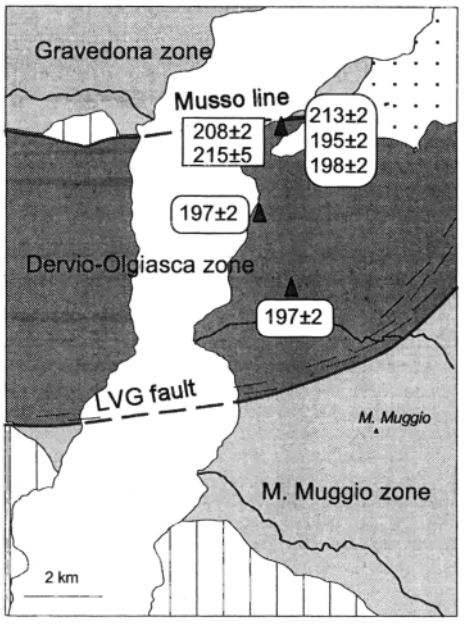

Figure 4. Rb/Sr ages. Frames with rounded corners indicate micaschist samples. Frames with nonrounded corners refer to determinations on pegmatites. LVG is Lugano-Val Grande fault.

than schists which is compatible with the higher closure temperature of feldspar with respect to that of muscovite. All obtained ages point to high temperatures around the initial stages of rifting.

3.2. Argon Geochronology

Samples were taken from all major domains of the area: from the Monte Muggio zone, from the Dervio-Olgiasca zone, and from the mylonites of the Lugano-Val Grande fault zone separating the two (Figure 5a). Both step heating and spot analysis experiments were performed.

3.2.1. Step heating. Incremental heating techniques have been used extensively on mineral separates and more recently on single crystals [e.g., *Layer et al.*, 1987; *Wijbrans et al.*, 1990] and are particularly powerful because the sample is tested for homogeneous radiogenic Ar content. Inhomogeneities can be interpreted in terms of loss or gain of Ar, which, in turn, may help to constrain the thermal history of the sample. In addition, single-crystal incremental heating has been used to assess variation in ages from a single sample [e.g., *Wright et al.*, 1991]. Age spectra were produced for all measured samples and subsequently interpreted in terms of integrated, primary, and overprinted ages (Figure 6 and Table 2).

Muscovites and biotites from the southernmost part of the profile (Figures 5 and 6) (samples Gi 373 and DB 9016) yield ages of 328-354 Ma. Samples farther to the north but still south of the Lugano-Val Grande fault zone, Gi388 and Gi 451, show a significantly different signature with ages of 198±5 Ma and 190±7 Ma, respectively. Mylonitic schists associated with the Lugano-Val Grande fault have muscovite ages between 222±8 Ma (Gi 453) and 204±7 Ma (Gi 445) and a significantly younger biotite age of 190±5 Ma (Gi 444). Hornblende from a mylonitized amphibolite from Monte Legnone (Gi 445) yielded a poor spectrum suggesting a cooling age of 204±7 Ma. Biotites and muscovites from the Piona peninsula (northernmost part of the Dervio-Olgiasca zone) yielded well-defined ages between 200±5 Ma and 191±0.5 Ma. We could detect no systematic difference between muscovite and biotite nor between the mica ages of the gneisses and those of the pegmatites outcropping in the area. One hornblende from an amphibolite layer yielded a more disturbed spectrum because of the incorporation of excess Ar. Its lowest age of 230 Ma is interpreted as a maximum estimate for the age of this hornblende.

Table 1. Results of Rb/Sr Radiometric Dating

Sample	Lithology	Mineral, mm	Rb	Sr	$^{87}Rb/^{86}Sr$	$^{87}Sr/^{86}Sr$	2σ	Age, Ma	±2σ
ST1	pegmatite	Ksp 0.5-1	33.1	173.2	0.5547	0.725702	0.000008	208	2
ST1	pegmatite	ms 0.5-1	463	13.44	102.8	1.028210	0.000017		
ST8	pegmatite	Ksp 0.1-1	103	14.15	21.29	0.810255	0.000014	215	2
ST8	pegmatite	ms 0.5-1	890	1.426	3948	12.8367	0.0011		
ST2	schist	ms 0.3-0.5	309	34.52	26.10	0.802594	0.000011	195	2
ST2	schist	bi 0.3-0.5	873	1.714	2464	7.57395	0.00012		
ST3	schist	ms0.25-0.5	230	27.34	24.53	0.799402	0.000011	213	2
ST3	schist	bi 25-0.5	705	2.350	1170	4.26171	0.00009		
ST4	marble	cal 0.3-0.5	0.139	139.1	0.0029	0.709257	0.000010	198	2
ST4	marble	ms 0.3-0.5	274	3.644	231.1	1.359854	0.000023		
ST5	schist	ms0.25-0.5	104	198.0	1.520	0.732482	0.000012	197	2
ST5	schist	bi0.25-0.5	591	4.246	453.2	1.99450	0.000032		
ST6	schist	ms0.25-0.5	172	248.8	2.01	0.733698	0.000009	197	2
ST6	schist	bi0.25-0.5	591	8.622	210.3	1.316807	0.000019		

Uncertainty in measured $^{87}Sr/^{86}Sr$ refers to least significant digits and represents ± 2σ run precision. Errors in ages have been calculated at 95% confidence level.

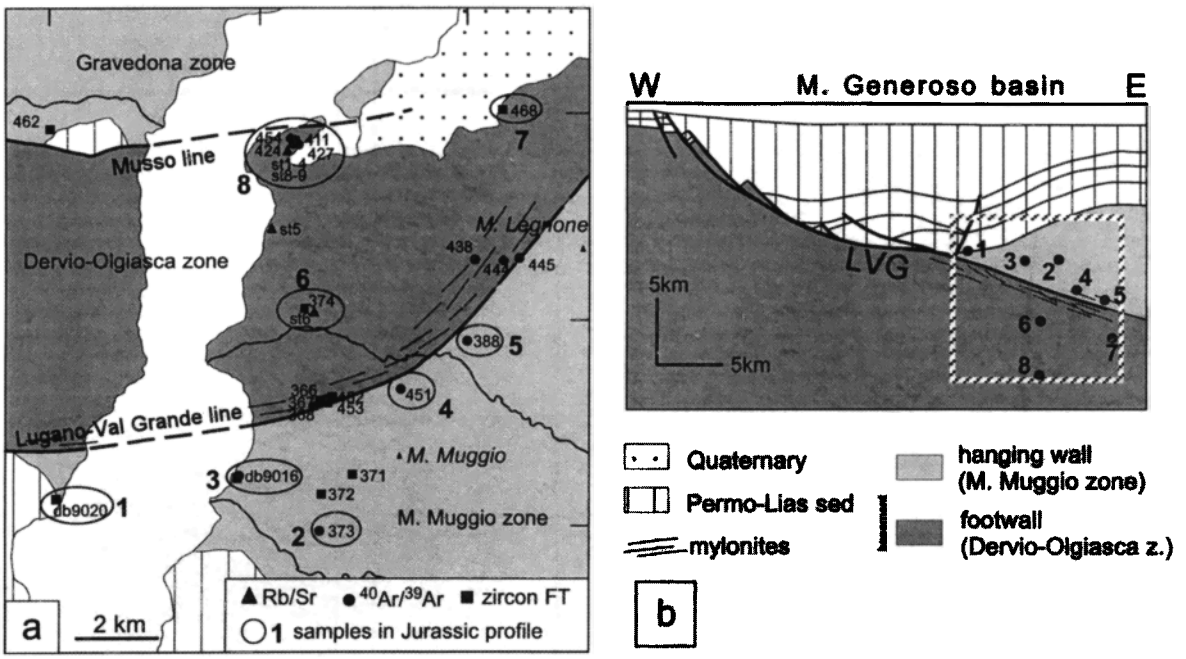

Figure 5. (a) Schematic geologic map of the northern Lake Como area with the sites sampled for absolute dating. Samples used for comparison with thermal modeling are circled and numbered. (b) Schematic cross section across the Monte Generoso basin in Jurassic times. The outlined square indicates the Jurassic position of the northern Lake Como region. Numbered points give the position in Jurassic times of the samples shown in Figure 5a.

Hence $^{40}Ar/^{39}Ar$ ages fall into two distinct groups with those older than 320 Ma lying in the southernmost part of the Monte Muggio zone. These ages are compatible with the only previously reported age (K/Ar) of 330±10 Ma [*Mottana et al.*, 1985] and are readily explained as cooling ages following the last stages of Variscan deformation [*Diella et al.*, 1992]. Other samples yielded ages between 220 Ma and 180 Ma with a poorly defined younging trend from south to north. The transition between the two groups occurs within the Monte Muggio zone. The Lugano-Val Grande fault zone does not separate domains with different ages, and ages of mylonite samples do not significantly differ from those of the adjacent rocks.

Most mica samples show partial disturbances of the argon system. These are interpreted as young overprint ages in the range of 100-140 Ma in the low-temperature steps (Figure 6 and Table 2) which could perhaps be linked to the first stages of Alpine exhumation or, less likely, to thermal reactivation during the Cretaceous.

3.2.2. Spot fusion. We analyzed up to 1-cm-large feldspar augens from the mylonites of the Lugano-Val Grande fault zone (Figure 5) with spot fusion techniques [*Phillips and Onstott*, 1988; *Hodges and Bowring*, 1995]. This approach was used because of the prolonged history of high-temperature deformation and crystallization and of the presence of biotite, muscovite, and quartz inclusions [*Bertotti*, 1991]. The clasts originate from mylonitization of an orthogneiss body locally preserved in the hanging wall of the Lugano-Val Grande fault [*El Tahlawi*, 1965; *Siletto et al.*, 1990]. Because of the complex poikiloblastic character of the feldspars, it was not possible to extract age information using conventional or laser incremental heating techniques. Particular attention has been devoted to lateral age variations within each grain and to minerals formed during deformation in pressure shadows of the larger crystals.

The results of spot fusion experiments are shown in Figure 7. The age pattern within each crystal is complex. In some cases, such as in experiments Gi 452/c and Gi 452/d there is a tendency for the older ages to be located toward the center of the grain. The pattern is, however, far from systematic, and crystals Gi 452/b and Gi 453, for instance, produced old ages (270-300 Ma) close to the edges. Their prolonged history of deformation is the most likely cause. Somewhat more consistent are the ages obtained from spots in the "tails" and pressure shadows of the crystals. In experiment Gi 452/b these points provided ages of 226±9.1 Ma and 184±1 Ma; biotites from similar positions in experiment Gi 452/d produced ages of 206±2 Ma and 197±1.2 Ma.

All spot fusion analyses were plotted as a histogram (Figure 8) to provide a crude first-order interpretation of the data. Most data points plot in the range 275-185 Ma with a peak at 220-230 Ma. Five points plot in excess of 275 Ma yielding signatures of Paleozoic events. None of the data plot below 185 Ma, that is, after the cessation of continental extension.

3.3. Zircon Fission Track Studies

With the exception of Gi 462 and DB 9020, samples for fission track analysis were collected along a profile E of Lake Como from the sedimentary cover in the south to the Musso Line in the north (Figure 5a). It was sometimes difficult to

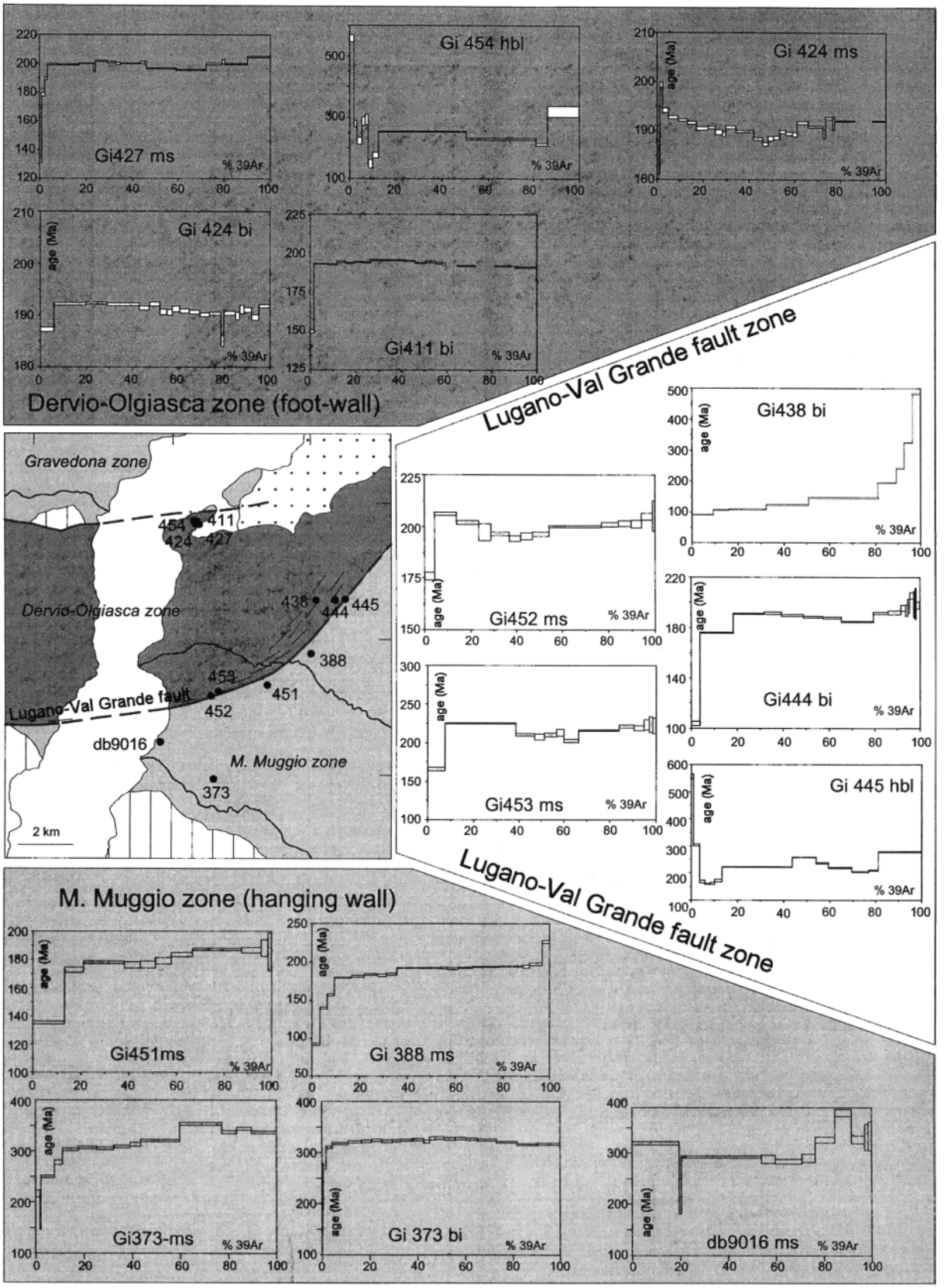

Figure 6. The $^{40}Ar/^{39}Ar$ age spectra derived from the northern Lake Como samples. Abbreviations are as follows: ms, muscovite; bi, biotite; and hbl, hornblende.

Table 2. Results of $^{40}Ar/^{39}Ar$ Incremental Heating Experiments

Sample	Mineral	Integrated Age, Ma	Primary Age, Ma	Overprint age, Ma	Interpretation
Gi 373	muscovite	321.7±0.9	354±10	~200Ma	partially overprinted
	biotite	326±0.9	328±10	<140	partially overprinted
DB 9016	muscovite	318±0.9	340±10	<300	
Gi 451	muscovite	178±1.0	190±7	<137	Ar loss pattern
Gi 388	muscovite	186±1.0	198±5	<92	partial Ar loss pattern, highest stages in final steps approach real age
Gi 452	muscovite	199±1.0	205±7	<176	partially disturbed with ages increasing toward a maximum in the second 65%
Gi 453	muscovite	214±1.0	222±8	<166	partially disturbed with ages increasing to maximum age in the final steps
Gi 444	biotite	185±1.0	190±5	<104	somewhat disturbed diffusion loss pattern
	muscovite	197±1.0	--	--	virtually undisturbed spectrum; no overprint age recorded because of large first step
Gi 445	hornblende	236±1.0	204±7	--	disturbed spectrum, excess Ar obscures primary age
Gi 438	biotite	155±1.0	>145	<90	Ar loss pattern, with severe overprinting anomalous ages in last four steps because of hornblende inclusions
Gi 411	biotite	194±1.0	194±5	<150	plateau age over 98%
Gi 424	muscovite	190±1.0	192±5	<168	somewhat disturbed spectrum with most ages in the 187-194 Ma range
	biotite	191±1.0	191±0.5	<187	slightly disturbed; integrated age is close to plateau age
Gi 427	muscovite	198±1.0	200±5	<133	plateau age close to integrated age
Gi 454	hornblende	236±1	204±8	--	disturbed spectrum, excess Ar obscures primary age

The integrated age is the age calculated over the total gas released. Primary age gives the best estimate for the original age of the mineral and should be interpreted as the age at which the mineral cooled below the Ar closure temperature. Overprint age is an interpretation of the results of the initial steps of the experiment under the assumption that least retentive mineral sites are fully degassed during a thermal resetting.

obtain well-constrained ages because of the scarcity of zircon grains in most samples.

Zircon fission track ages from northern Lake Como lie between 223 Ma and 49 Ma (Figure 9 and Table 3). Zircon ages in the Monte Muggio zone are 176±29 Ma (DB 9020), 177±34 Ma (Gi 371), and 151±31 Ma (DB 9016), statistically identical. Sample Gi 372, for which only few grains could be measured, produced an age of 223±40 Ma. Samples from the mylonites of the Lugano-Val Grande fault zone yielded poorly defined yet statistically equivalent ages between 161 Ma and 135 Ma. Farther to the north, an age of 139±28 Ma was measured on a sample from the Dervio-Olgiasca zone. The northernmost sample south of the Musso Line provided a well-constrained and very important result of 49±7 Ma. Overall, ages south of the Musso Line show a younging trend toward the north from 223±40 Ma to 49±7 Ma. All but the 49 Ma age are rift- or drift-related ages. The 49 Ma age falls into the time of Alpine contraction.

North of the Musso Line (sample Gi 462), ages are of 210±84 Ma and comparable to those obtained from the Monte Muggio zone which is compatible with the upper crustal position of the rocks north of the Musso Line during the Mesozoic [*Bertotti et al.*, 1993b].

4. Crustal Thermal Evolution

Most of the ages we have obtained fall close to, during, or after the main period of crustal extension which has been constrained between the Early Norian (220 Ma) and the Late Liassic (186 Ma) by the sedimentary record [*Bertotti et al.*, 1993a]. During this time the Lugano-Val Grande normal fault was active causing substantial vertical displacements between

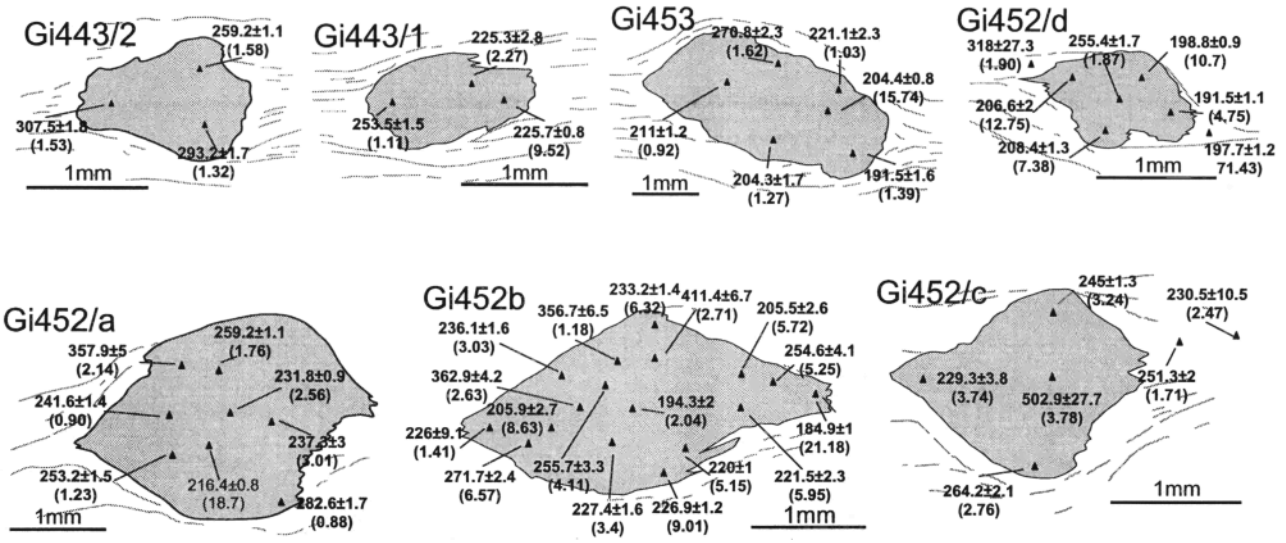

Figure 7. Results of spot fusion analysis on porphyroblasts of the Lugano-Val Grande mylonites.

the hanging wall (Monte Muggio zone) and the footwall (Dervio-Olgiasca zone) thereby opening the Monte Generoso rifted basin (Figures 2 and 3).

Absolute ages provide estimates for the moment when the sample has cooled below the closure temperature of a given geochronological system. Since such a cooling can be caused both by an upward movement of the sample and/or by a downward movement of the isotherms relative to the Earth's surface, the kinematics of the samples must be independently assessed before absolute ages can be used to obtain information on the thermal field. This is unavoidable if, such as in our case, absolute ages fall within a period of intense deformation. In section 4.1, we shall describe the kinematics of the rifted system and use the absolute ages to derive a reconstruction of the thermal structure of the Monte Generoso crustal segment prior to, during and after rifting.

4.1. Mass Movements: The Kinematics of the Monte Generoso Crustal Segment in the Mesozoic

In order to constrain the kinematics of the samples during the Mesozoic, that is, during the time span recorded by the absolute ages, two kinds of data are needed: (1) the position of the sample points prior to Alpine contraction which brought them into the present-day position and (2) the kinematics of fault-block movements prior to and during rifting.

The position of the sample points in the pre-Alpine, postrift section (Figure 5) is geometrically reconstructed by measuring their present-day distances from the sediment/basement contact and from the Lugano-Val Grande normal fault under the assumption that no major Alpine fault disrupted the Lake Como section from the Triassic sediments in the south to the Musso Line in the north (Figure 3). None of the many studies carried out so far in the area has demonstrated such a disruption [e.g., *Siletto et al.*, 1990; *Bertotti*, 1991]. On this basis, samples are placed in the section of Figure 5.

The Mesozoic kinematics of the various parts of the Monte Generoso crustal segment are well constrained by the exten-

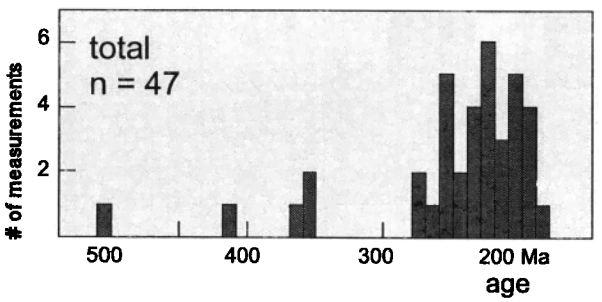

Figure 8. Histogram of the spot fusion results given in Figure 7.

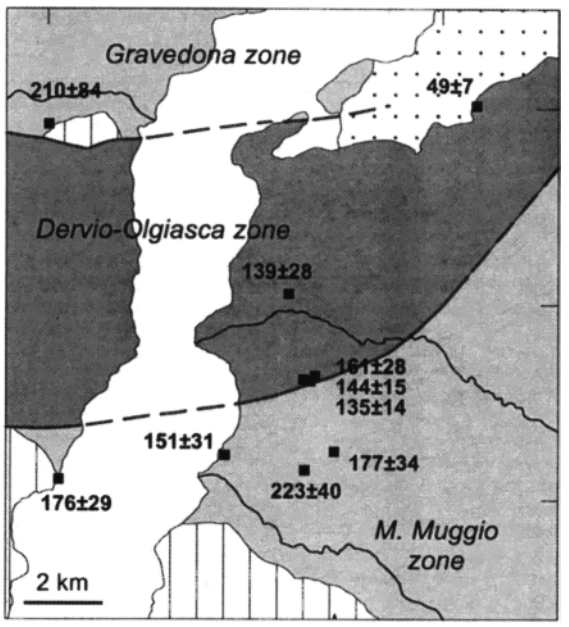

Figure 9. Zircon fission track ages. Errors are 2σ.

Table 3. Results of Fission Track Analysis

Sample Number (Laboratory / Irradiation Number)	Grains Counted	Standard Track Density x 10^4 cm^{-2} (Counted)	ρ_S x 10^4 cm^{-2} (Counted)	ρ_i x 10^4 cm^{-2} (Counted)	$P(\chi^2)$ %	Central Age ± 2σ, Ma
Gi 462 (eth-29)	6	14.0 (2174)	15.2 (859)	1.5 (86)	<1	210 ± 84
Gi 468 (eth-29)	11	14.0 (2174)	10.2 (1089)	4.84 (517)	3.8	49.4 ± 7.4
DB 9016 (eth-16)	8	128 (1268)	1578 (867)	222 (122)	89	151 ± 31
DB 9020 (eth-16)	17	12.8 (1268)	1767 (2722)	228 (351)	<1	176 ± 29
Gi 366 (ALP 245)	11	37.8 (5227)	1338 (1150)	189 (162)	40	161 ± 28
Gi 367 (ALP 246)	18	37.8 (5280)	1304 (2873)	207 (455)	30	144 ± 15
Gi 368 (ALP 247)	20	38.0 (5258)	1254 (3024)	214 (515)	30	135 ± 14
Gi 371 (ALP 250)	8	37.7 (5258)	992 (976)	127 (125)	80	177 ± 34
Gi 372 (ALP 251)	10	37.6 (5258)	1310 (1471)	133 (149)	40	223 ± 40
Gi374 (ALP 253)	7	37.6 (5258)	769 (735)	126 (120)	30	139 ± 28

All samples were irradiated at the Australian Nuclear Science and Technology Organisation facility, Lucas Heights, Australia. Ages were calculated using the zeta approach [*Hurford and Green*, 1983]. Errors are calculated according to *Green* [1981]. Values ρ_S and ρ_i represent sample spontaneous and induced track densities; $P(\chi^2)$ is the probability of obtaining χ^2 for ν degrees of freedom where ν = number of crystals - 1. Value $\lambda_D = 1.55125 \times 10^{-10}$. Zeta for eth irradiations=338±5 and 122 ±15 for all others.

sively studied sedimentary record of both hanging wall and footwall (Figure 3b). During Early Triassic to Carnian times (250-220 Ma) the Paleozoic basement of the entire area subsided roughly uniformly by <1000 m. This estimate is applicable to the entire crustal segment given the absence of major faulting during this time span [*Brack and Rieber*, 1993]. Normal faulting along the Lugano-Val Grande normal fault began in the Norian (220 Ma) and continued until the Late Liassic (~185 Ma). During this time interval the hanging wall of the Lugano-Val Grande fault subsided by 8-10 km. This magnitude is constrained by the decompacted thickness of the sediments filling the Monte Generoso basin [*Bernoulli*, 1964; *Bertotti*, 1991]. During this same time interval a few hundred meters thick sedimentary succession was deposited on the footwall under increasing water depths estimated at several hundred meters. Following the end of extension the entire crustal segment underwent gentle thermal subsidence and less than a few hundred meters of sediments were deposited in a pelagic environment [*Bernoulli*, 1964; *Winterer and Bosellini*, 1981]. Subsidence and thermal modeling [*Bertotti*, 1991; *Bertotti et al.*, 1997] suggest a limited depth increase of the order of <1000 m.

4.2. Movements of Rocks and of Isotherms: An Integrated Diagram

In Figure 10 we have plotted independently the vertical component of the movements experienced by the sample points prior to and during rifting as well as the results of absolute age determinations. Paleobathymetries have been neglected since they do not affect significantly the thermal structure of the underlying crust. The kinematics of footwall and hanging wall points are fairly well known and have been described in section 4.1. It is more difficult to track vertical movements for points within the Lugano-Val Grande fault zone because their original position and the moment of incorporation in the fault zone itself are not known. In any case, only downward movements are expected with the amount of displacement bracketed between zero and the total displacement of the hanging wall. Combining kinematic reconstruction and absolute ages, the thermal evolution of each material point can be reconstructed.

4.2.1. Hanging wall. Rocks in the upper part of the hanging wall (samples Gi 373 and DB 9016) descended by > 5 km but were never heated above the $^{40}Ar/^{39}Ar$ closing temperature and therefore preserve their Variscan isotopic signature. Together with DB 9020 they were, however, heated above the zircon annealing temperature. Originally deeper samples (Gi 388 and Gi 451) have younger ages which suggests that they were heated above the $^{40}Ar/^{39}Ar$ closing temperature and subsequently, during and despite their downward movement, cooled below the same temperature range at around 200 Ma. Temperatures after 200-190 Ma were never high enough to reopen the $^{40}Ar/^{39}Ar$ radiometric clock. Cooling through the $^{40}Ar/^{39}Ar$ closing temperature took place during the hanging wall downward movement. Zircon fission

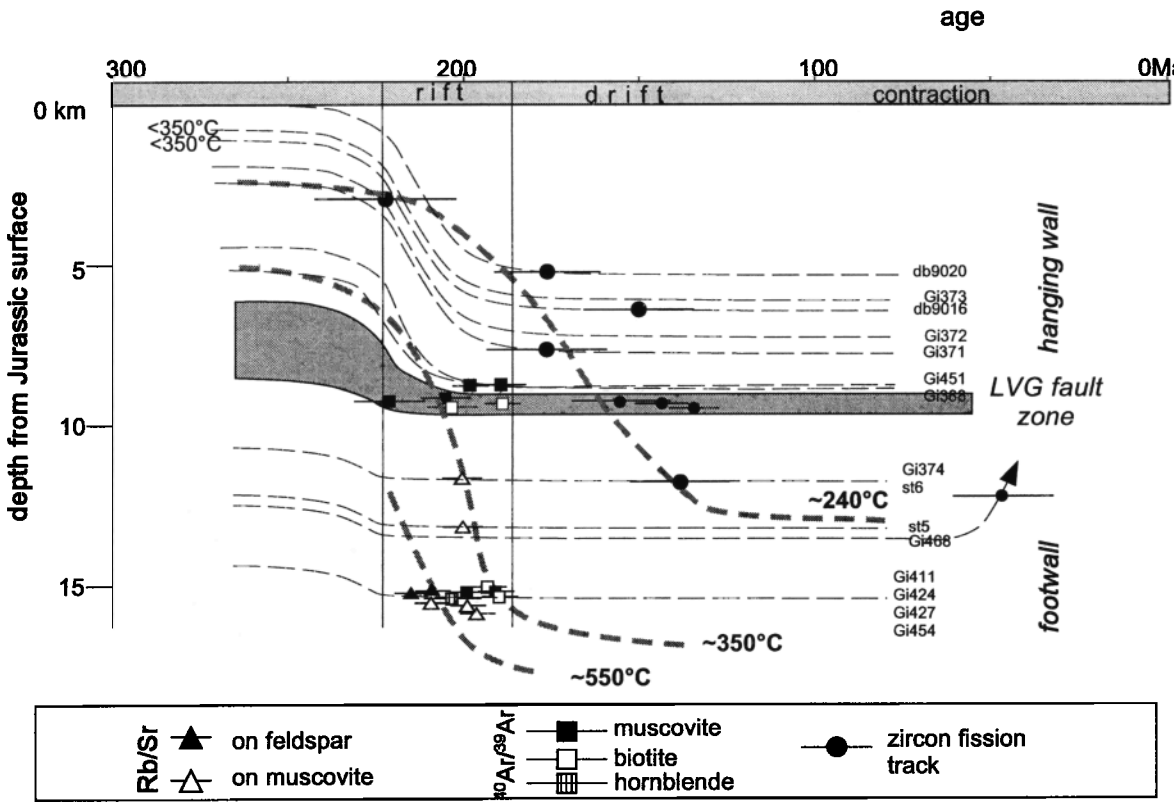

Figure 10. Diagrammatic view of the thermokinematic evolution of the northern Lake Como rocks. Note that the vertical movements of the various material points are determined only on the base of the overlying sedimentary record and carry no implicit assumptions on thermal gradients.

track ages are somewhat scattered but demonstrate that cooling continued throughout the Jurassic and that the samples were below the zircon annealing temperatures at approximately 160-180 Ma.

4.2.2. Fault zone. Fault zone samples passed the $^{40}Ar/^{39}Ar$ closing temperature at around 200 Ma, that is, during their downward movement within the Lugano-Val Grande normal fault. Results of spot fusion analysis on mylonite clasts within the Lugano-Val Grande fault zone are quite scattered. However, most of the ages fall in the 230-180 Ma range which overlaps with those ages obtained by step heating techniques. Minerals in pressure shadow zones which formed during deformation do not differ significantly from the mentioned range. Hence cooling through the closing temperature took place sometime between 230 and 180 Ma. Zircon fission track data suggest that cooling continued following the end of rifting and that around 150 Ma the rocks were at temperatures below the annealing temperature.

4.2.3. Footwall. Rb/Sr on feldspars and $^{40}Ar/^{39}Ar$ an amphiboles data provide concurring evidence that temperatures of $\geq$ 500°C were present in the deeper parts of the section at about 220-215 Ma. The $^{40}Ar/^{39}Ar$ ages on micas indicate that by 210-190 Ma temperatures in the same crustal levels had already decreased to ~350°C. The continuation of the trend is demonstrated by the Late Jurassic to Early Cretaceous age measured on zircons of sample Gi 374. Cooling, however, did not continue further, and the deepest part of the section represented by sample Gi 468 remained at temperatures above the zircon annealing temperature. During this entire time span the rocks did not experience large vertical movements. Alpine exhumation in Eocene times is demonstrated by the age of sample Gi 468.

4.3. Thermal Configuration of the Monte Generoso Crust Prior to, During, and After Rifting

The geological evidence demonstrates that none of the samples analyzed for absolute ages had undergone substantial upward movement in the time range covered by the obtained ages, that is, before Alpine contraction. It is thus an inescapable conclusion that movement of masses cannot explain the cooling experienced by the samples and that the closing of the isotopic system must be interpreted in terms of movements of isotherms.

To (semi-) quantify these changes, we have constructed representative isotherms assuming that at the time given by an absolute age the temperature of the sample corresponded to the closing temperature for a given system. In the depth versus time diagram of Figure 10 therefore a line connecting the absolute ages of a given system of all samples roughly represents an isotherm. In the diagram we have plotted three isotherms: the 550°C isotherm is roughly representative of Rb/Sr on feldspars and $^{40}Ar/^{39}Ar$ on amphiboles closing temperatures; the 350°C isotherm roughly corresponds to the $^{40}Ar/^{39}Ar$ closing temperatures on micas [*von Blanckenburg et al.*, 1989], and

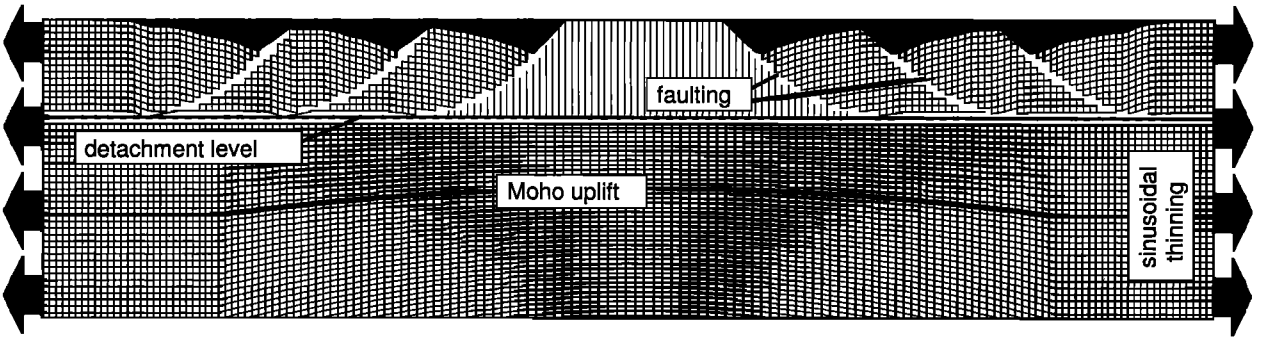

Figure 11. The geometric setting of the thermal-kinematic model.

the 240°C isotherm is taken as representative of zircon annealing temperatures [*Yamada et al.*, 1996]. We are aware of the variability of closing temperatures and of all problems associated with this concept. The depicted isotherms are therefore merely intended to provide a first-order description of the evolutionary trends.

Strongly perturbed thermal conditions are observed in the Lake Como crustal section around 230 Ma. Thermal gradients at this moment must have been >40°-60°C km^{-1}. Only the uppermost few kilometers of the crust were cooler than the zircon fission track annealing temperatures, and samples lying at 4-5 km depth (e.g., Gi 451) were above the $^{40}Ar/^{39}Ar$ closure temperatures. At ~15 km depths, rocks were not far from melting conditions, and high-temperature static metamorphism took place as shown by rocks of the Piona region [*Sanders et al.*, 1996].

From ~220 Ma, roughly contemporaneously with the onset of rifting, thermal gradients decreased substantially despite the onset of rifting. At 180-190 Ma, when extension in the Lombardian basin had come to an end, thermal gradients were of the order of 25°-30°C km^{-1} and around 150 Ma they had decreased down to ~20° C km^{-1}. The entire upper 12 to 13 km thick crustal section was below the zircon fission track annealing temperature. The rock originally at depths >13 km remained above 240°C. This thermal situation remained stable until Alpine contraction when the rocks of the Lake Como section were exhumed.

5. Numerical Modeling and Absolute Ages

In the following we apply thermal-kinematic numerical modeling techniques to predict the synrift and postrift thermal evolution of the Monte Generoso crustal section. We then extract from the model synthetic temperatures-time (T-t) curves for representative localities and compare them with the data obtained from absolute age determinations

5.1. Model and its Input

A new numerical model describing the kinematics and thermal evolution of rifted basins has been developed recently [*ter Voorde and Bertotti,* 1994] and has been used to study thermal changes associated with normal faulting. The model allows for a two-dimensional, time-dependent description of crustal extension and satisfies the volume preservation condition. It has an upper part where extension is accommodated along discrete faults and a lower one where extension is distributed (Figure 11). Temperatures are calculated by a finite difference method on a rectangular grid. Thermal properties on each point are obtained by interpolation from a second, moving grid representing the extending basin. The thermal model includes heat production and differences in heat conductivity values for different materials such as sediments or basement rocks. Values adopted are shown in Table 4.

The evolutionary scheme used in the model is based on the geological evidence presented above. To reproduce the strongly perturbed thermal conditions at 230 Ma, a 100-km-wide intrusion was placed at 30 km depth with a temperature of 1000°C [*Bertotti et al.*, 1997]. At 7 Ma after emplacement (i.e., at 223 Ma) the heat source is "turned off". Normal faulting and crustal thinning begin at the same time as constrained by the field data. Extension kinematics follow the time scheme shown in Table 5, and stretching terminates 37 Ma after the onset of rifting (i.e., at 186 Ma) [*Bertotti et al.*, 1993a; *Bertotti and ter Voorde,* 1994]. The model includes thermal-kinematic effects of all faults active in the South Alpine rifted margin (Table 5). The thermal field during rifting results from the interactions of rift-related mass movements and effects of the magmatic intrusion.

5.2. Results of Modeling

The modeled thermal evolution of the Monte Generoso basin crustal section is shown in Figure 12. Thermal conditions at the onset of rifting (Figure 12a) are strongly disturbed because of the presence at depth of a magmatic intrusion. Temperatures at 15 km depth, roughly corresponding to the Piona samples (point 8 in Figure 12), are predicted at 650°-700°C. These values are compatible with pressure-temperature estimates derived from very similar rocks [e.g., *Diella et al.*, 1992; *Sanders et al.*, 1996]. Once the heat source is "turned off," the isotherms rapidly relax. Already 13 Ma later and despite the active extension, thermal gradients of 25°-30°C km^{-1} are predicted. At the end of activity of the Lugano-Val Grande fault, isotherms are virtually flat and gradients of 20°-25°C km^{-1} are expected from the model. Very few changes occur afterward, in the postextensional stage.

In general, the model predicts that the thermal evolution of the Monte Generoso crust is substantially controlled by the waning of the thermal anomaly and that continental rifting taking place at the considered rates (~10^{-16}s^{-1}) [*Bertotti et al.*, 1993a] did not provide any significant contribution. Even at the end of rifting, that is, at the moment of highest crustal

stretching, there is a limited distortion. It is also observed that normal faulting causes little or no disturbance of the isotherms. Isotherms tend to cross the fault zone undisturbed, and no footwall cooling is observed because of the downward movement of the hanging wall [cf. *Bertotti and ter Voorde,* 1994].

To follow more clearly the thermal evolution of the various parts of the system, we have extracted from the model synthetic T-t curves for points representative of the Mesozoic position of the localities which have been sampled for absolute age determinations (Figure 13).

T-t paths for the hanging wall reflect the combined effects of heating and subsequent cooling of the thermal anomaly and of synrift heating due to the downward movement of the hanging wall. The predominance of one or the other process depends on the distance of a particular point from the thermal anomaly. The simplest path is shown by point 1 which was at the surface at the onset of rifting and therefore is maintained at constant temperature until this moment. With the onset of extension, it moves downward and is progressively heated. A component related to the thermal anomaly is present. In points 2 and 3, heating starts before the onset of extension in association with the intrusion and continues throughout rifting although at a decreasing rate. Subsequently, the downward movement of the points progressively overshadows the thermal effects of the intrusion, which were dominant in the initial stages. After breakup, cooling by a few tens of degrees is predicted. The T-t path of points 4 and 5, which were deep, is clearly dominated by the intrusion-related component. Highest temperatures are already reached in the initial stages of rifting. Further, the kinematics-controlled temperature increase is small because of the limited amount of downward movement experienced by the points.

Footwall points show very large temperature changes through time, with amplitudes increasing with depth. Since these points did not move significantly in the vertical direction, thermal changes must be associated with the effects of the thermal anomaly. About 90% of the cooling is completed before the end of extension. The component related to lithospheric thinning is therefore very small. After thermal relaxation, temperatures are somewhat higher than before the onset of thermal perturbation and of extension. This is due to the cumulative effects of sediment blanketing and heat production [*ter Voorde and Bertotti,* 1994].

5.3. Comparison With Measured Absolute Ages

On the synthetic T-t curves of Figure 13 we have plotted the absolute ages for the various chronological systems. By doing this, we derive estimates for the temperature of a sample point at the moment it was cooled below the closing or annealing temperature of a given chronological system.

Estimated $^{40}Ar/^{39}Ar$ closing temperatures generally increase with increasing depth. For the most superficial samples with Mesozoic ages, Gi 451 (point 4) and Gi 388 (point 5), micas $^{40}Ar/^{39}Ar$ closing temperatures of ~250°C are predicted which are clearly lower than usually assumed [e.g., *von Blanckenburg et al.,* 1989]. For deeper samples, such as those of point 8, temperatures of 300°-350°C are calculated which are in line with those generally adopted. Predicted closing temperatures for hornblende are rather on the low side, but the T-t curve in this region is very steep, and even small changes in model pa-

Table 4. Parameters used in Thermokinematic Modeling

Parameter	Value
T at surface	25°C
T at base lithosphere	1330°C
Thickness heat-producing layer	15 km
Heat production in layer	2.3×10^{-6} W m^{-3}
Specific heat	1100 J kg^{-1} K^{-1}
Thermal diffusivity in sediments	0.75×10^{-6} m^2 s^{-1}
Thermal diffusivity in basement	10^{-6} m^2 s^{-1}

Model parameters are from *ter Voorde and Bertotti* [1994].

Table 5. Kinematics of the Four Major Normal Faults of the South Alpine Margin

Fault	Extension Rates, mm yr^{-1}	
	0-13 Ma	13-37 Ma
Lago Maggiore	0.23	0.09
Lugano-Val Grande	0.78	0.22
Sebino	0.32	0.06
Garda	0.16	0.10

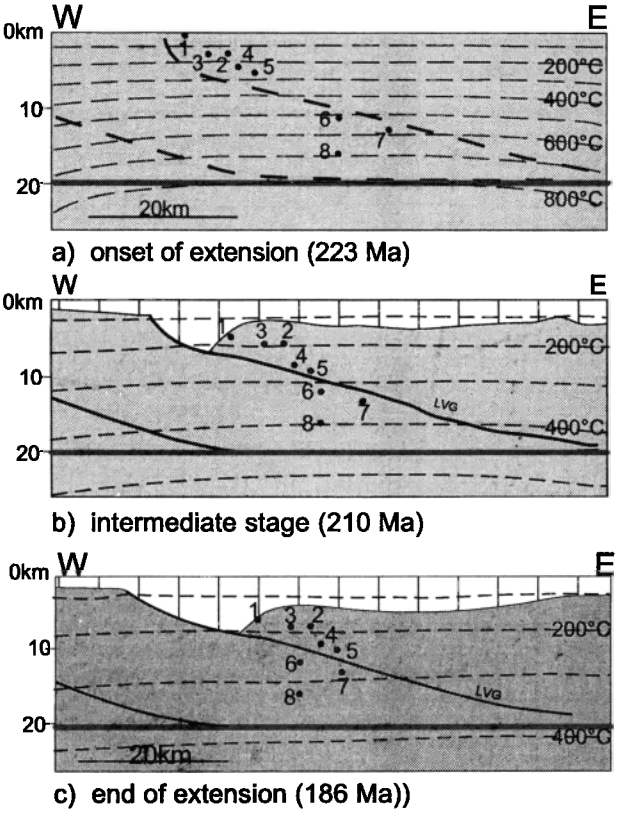

Figure 12. Results of thermal kinematic modeling of the Monte Generoso section during and after rifting: (a) onset of extension, (b) intermediate stage, and (c) end of extension. Points indicate paleoposition of samples taken for absolute age dating. The thick horizontal line is the detachment horizon shown also in Figure 11.

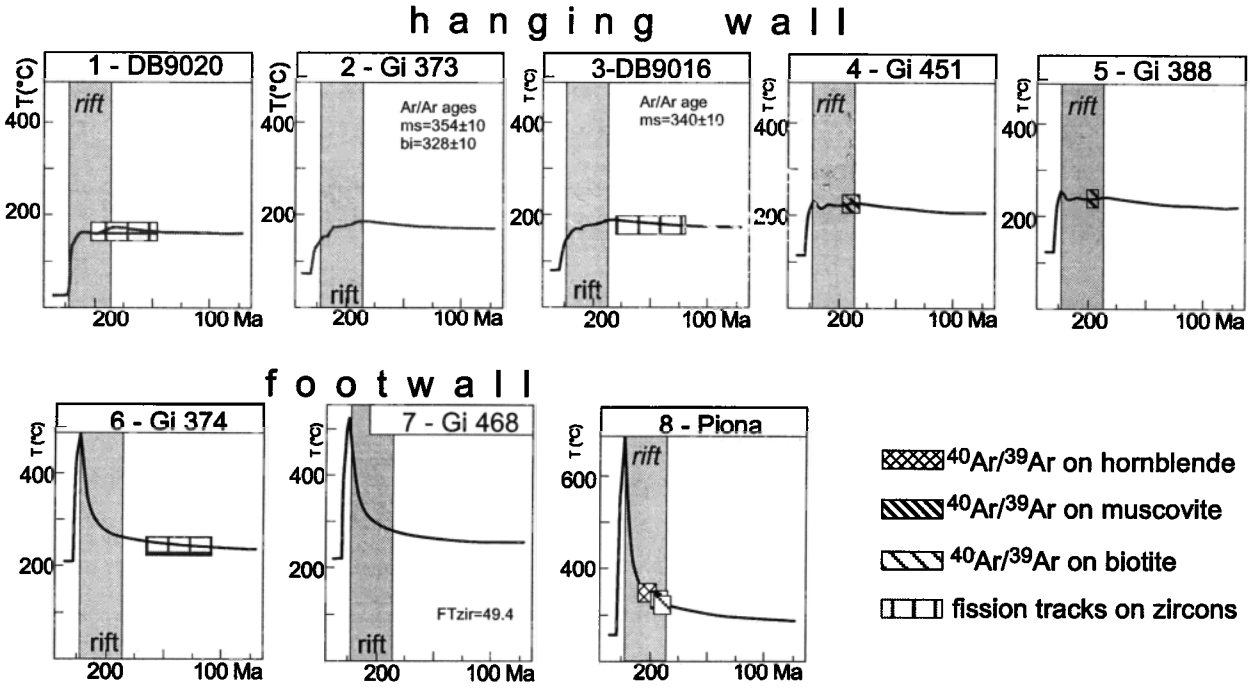

Figure 13. Synthetic temperature-time curves and absolute ages for selected points of the system (see Figures 5 and 12 for their Jurassic position in the section and in the model, respectively). The various absolute ages are plotted as bars, the length of which is proportional to the measurement error. Ages which could not be plotted within the horizontal scale adopted are indicated in each box. Note the different vertical scale for the box of point 8 (Piona).

rameters or in the data could immediately bring about a higher temperature.

Annealing temperatures for zircons derived from our curves are around 180°C in the uppermost samples (DB 9020 and Gi 373). They increase with depth and are ~220°C for sample Gi 374 (point 6). Although also on the low side, these temperatures fall within the range of *Yamada et al.* [1996]. The T-t curve for the slightly deeper sample Gi 468 is always above 250°C which is compatible with its zircon FT age of 49 Ma. All synthetic T-t curves predict Mesozoic temperatures higher than 150°C and are therefore compatible with unpublished apatite fission track data which are systematically Alpine.

In general, it seems that predicted closing/annealing temperatures are lower than generally assumed in the upper crustal levels but become more and more compatible toward deeper crustal levels. This discrepancy could point to difficulties of the model in producing high thermal gradients, that is, high temperatures at shallow crustal levels. Despite all uncertainties associated with our modeling procedure and with the parameters adopted, the thermal evolution predicted by the model is quite robust. This is particularly true for the uppermost kilometers of the crust which are quite insensitive even to large variations of heat source parameters at depth. Numerical experiments have shown, for instance, that a 200°C increase of the temperature of the lower crustal heat source causes a warming of the order of a few tens of degrees in the upper crust.

6. Discussion

Our data have shown that isotherms in the Monte Generoso and surrounding crustal segment were strongly disturbed before the onset of continental extension in the Norian. The anomalous thermal configuration has been attributed to a Middle Triassic thermal anomaly [*Ferrara and Innocenti,* 1974; *Mottana et al.,* 1985] possibly related to the emplacement of a major magmatic body in the lower crust [*Bertotti and ter Voorde,* 1994; *Sanders et al.,* 1996]. The intrusion, which caused secondary melting and the formation of the pegmatites exposed in the Piona region (Figure 1) [*Sanders et al.,* 1996], is presently not preserved since the upper 15 km of Mesozoic crust have been detached from their substratum during Alpine contraction [e.g., *Schumacher et al.,* 1997]. Possible remnants, however, could be represented by magmatic pebbles found in the South Alpine Molasse which have yielded enigmatic Middle Triassic K/Ar ages (J.C. Hunziker, personal communication, 1995). Major thermal events taking place in the lower crust of the Southern Alps during the same time span have been postulated by *Vavra et al.* [1996]. Indeed, it has been proposed that the entire Pangean domain was in a strongly perturbated thermal state during the Middle Triassic [*Veevers,* 1989].

The presence of high thermal gradients already at the onset of rifting is not unique to the South Alpine case and has been postulated, for instance, by *Spadini et al.* [1995] for the Tyr-

rhenian Sea, by *Hendrie et al.* [1993] in the North Sea, and by *Foster and Fanning* [1997] for the Bitterroot core complex. One can speculate on possible causal relations between magmatism and thermal anomaly on one side and the onset of rifting on the other. This study has shown that the thermal anomaly was present (slightly?) before the onset of rifting and that the beginning of cooling and of extensional faulting broadly overlapped in time. In this case a key role of magmatism in softening the lithosphere allowing for the initiation of deformation could be envisaged. Rheological modeling [*Kusznir and Park,* 1987; *Lynch and Morgan,* 1987] as well as geological studies [e.g., *Nicolas et al.,* 1994] underline the hypothesis that tensional stresses can hardly cause any significant deformation unless lithospheric gradients are high and Moho temperatures are elevated above normal (>700°C).

Following the disappearance of the thermal anomaly, the Mesozoic thermal evolution of the Lombardian crust was substantially controlled by the relaxation of the isotherms. Rift-related block movements and lithospheric thinning did not provide any significant contribution. This picture only changed in the Late Cretaceous (?) and Tertiary with the onset of Alpine contraction. Synrift cooling had important consequences for the overall tectonic evolution of the South Alpine margin: (1) It imposed strong subsidence during the initial stages of rifting, that is, during a time span when only limited vertical movements are predicted by simple rifting models, (2) Coupled with the upward movement of mantle rocks associated with crustal thinning, it caused the strengthening of the lithospheric segment and eventually caused the lateral shift of the extension site known from the geological record [*Bertotti et al.,* 1993a], (3) It provoked a change in the deformation mechanisms with which the deeper parts of the extensional faults, such as the Lugano-Val Grande fault, operated. Strain rate-sensitive and temperature-sensitive mechanisms were replaced by brittle, pressure-dependent processes. For instance, the reconstruction presented (Figure 10) and the modeling study (Figure 12) suggest a synrift cooling from ~450° to 250°C for a hypothetical point located at ~12 km depth. Indeed, profiles across those deep parts of faults show mylonitic rocks being progressively overprinted by ultramylonites and cataclasites [*Bertotti,* 1991; *Bertotti et al.,* 1993b]. In contrast with "core complex" settings, this pattern is not due to an exhumation of the footwall.

7. Conclusions

During the Norian (~220 Ma), when the South Alpine rifting began, the geothermal gradient was higher than normal. Onset of cooling roughly coincided with the first appearance of extensional faulting and continued, at ever decreasing rates, during rifting and drifting. Fault blocks moved only downward and had no major influence on crustal thermal evolution. The same can be said for lithospheric thinning which provided little noticeable heating. As a consequence, absolute ages in the area are primarily controlled by the downward movement of isotherms and are not directly related to deformation. The tectonic interpretation of absolute ages is difficult when the crustal thermal and kinematic evolution of the crust is not well constrained and, as in the Monte Generoso case, when strong cooling is contemporaneous with deformation.

Cooling continued after breakup, but the residual thermal anomaly was so limited that the decrease in temperatures at middle crustal depths can be estimated at some tens of degrees. With the onset of Alpine contraction, the upper to middle crust was detached from its substratum along the Musso Line and brought into a steep south dipping position. Step heating and spot fusion results as well as geological observations demonstrate that no major reactivation occurred during this time span.

Appendix: Dating Techniques and Procedures

A1. Rb/Sr

Mineral separation was carried out by conventional magnetic and specific gravity techniques. The final separated mineral fractions were checked for purity and freshness by handpicking under a binocular microscope. Rb/Sr isotope dilution and Sr isotope composition analyses were performed from single sample dissolution, following digestion in PFA screw-top vials using an HF-HNO_3 mixture. After 4-5 days the samples were evaporated to dryness and were then completely soluble in hot 6N HCl. Roughly 20% of the solutions were spiked using mixed ^{87}Rb-^{84}Sr spikes. The total procedural blank for Sr was <200 pg at the time of these analyses. Isotopic ratios were measured on a Finnigan MAT 261 thermal ionization mass spectrometer equipped with nine fixed Faraday collectors. Sr isotope compositions were measured in dynamic mode and are presented normalized to $^{86}Sr/^{88}Sr=0.1194$. Uncertainties in $^{87}Sr/^{86}Sr$ refer to the least significant digits and represent +2 standard deviation run precision. Uncertainties (2 standard deviation) in Rb/Sr are <1%. The external precision of National Institute of Standards and Technology (NIST) SRM987 was $^{87}Sr/^{86}Sr=0.710278+18$ (2 standard deviations, n=26). For isochron calculation a minimum uncertainty of +0.00254% was assumed for the measured $^{87}Sr/^{86}Sr$, based on the external precision of NIST SRM987. If the standard error of an analysis (2σ run precision) was >0.00254%, then the higher value was used. Isochron regression was calculated with the software ISOPLOT [*Ludwig,* 1994], and age estimates are at the 2σ confidence level.

A2. $^{40}Ar/^{39}Ar$ Step Heating

For the incremental heating technique, hand specimens were crushed, and minerals were selected from the 250 to 500 μm fraction after removal of the dust fraction and preconcentrating the desired minerals, hornblende, biotite, and muscovite, with heavy liquids and a Faul table. Single minerals or small amounts of mineral of smaller grain size were loaded in 20 mm diameter Al sample trays which typically contain 16 experiments and four flux monitors. The experiment was packaged in a weld-sealed Al capsule and irradiated for 12 hours in the Training Research Isotope General Atomic Reactor (TRIGA) of Oregon State University (see *Wijbrans et* al. [1995] for further details). Taylor Creek Rhyolite sanidine (85G003, age 27.92 Ma) was used as a flux monitor. Incremental heating experiments were carried out with a laser beam focused to ~2 mm diameter to insure even heating of the entire

sample. A Continuous Wave-argon ion laser with a maximum energy of 18 W in all line modes was used. A typical incremental heating experiment consisted of 1-min laser heating of the sample followed by 4 min of cleaning of the gas in the inlet line. During the experiments on micas it was sometimes difficult to predict the amount of gas released per step. In the later stages of the project we modified the procedure to let in ~0.3 fraction of the gas before letting in the full amount. The 90-s inlet and equilibration time was sufficiently long to both carry out the peak centering routine on ^{40}Ar and check the intensity of the ^{39}Ar signal. Unfortunately, some of the age information (but not the ^{39}Ar fraction information) of large steps was lost in the early stages of the project because of saturation of the preamplifier.

A3. $^{40}Ar/^{39}Ar$ Spot Fusion

Approximately 90 μm-thick sections (20-mm maximum diameter) without glass backing and polished on one side were prepared for the spot fusion experiments (performed at the Vrije Universiteit, Amsterdam). We chose a 90 μm thickness because the average grain size is larger than 90 μm and thus fusing of any underlying crystals can be avoided. Sections are also transparent under the binocular zoom microscope, which facilitates identification of minerals. Thin sections were wrapped individually in Al foil with a 22-mm-diameter Al disc backing to prevent fragmentation in the irradiation capsule. Flux monitors were packaged between the individual thin section packages and loaded together with their Al tray backing. The laser beam was focused to ~20 μm diameter. Several short (0.1 s) pulses of 1.2 to 1.5-W laser energy fired at the sample over ~30 s time caused melt pits varying between 20 and 50 μm in diameter depending on energy absorption. Longer pulses tend to cause excessive heating around the laser spot. Silicate melt glass from the laser pit is deposited on the surface of the thin section around it.

Mass spectrometric (MS) techniques are documented elsewhere [*Wijbrans et al.*, 1995]. MS discrimination factor was determined at 1.0047 per mass unit, the Secondary Electron Multiplier was operated at a gain of 10,000, and system blanks were measured before and after each block of five unknowns. It was found that good results could be obtained from experiments on K-rich feldspar which contains high concentrations of radiogenic argon. When inadvertently K-poorer phases such as plagioclase or quartz inclusions were hit, the beam intensity was much lower. Results on K-feldspar were selected using beam intensity and K/Ca ratio (>1.0) as filtering criteria.

A4. Fission Tracks

Zircon was dated as outlined by *Seward* [1989] using the external detector method [*Gleadow*, 1981]. All ages are central ages and were calculated using the zeta factor approach [*Hurford and Green*, 1983] with a mean zeta value of 338±5 for dosimeter glass SRM962 and the Fish Canyon Tuff zircon (eth samples) and 122±15 for all others. Irradiations were carried out at the Australian Nuclear Science and Technology Organization facility. The statistical uncertainties on the ages are the standard error as defined by *Green* [1981] and incorporate errors from the induced and spontaneous tracks as well as those of the glass standard. Errors are expressed in million years at the 2σ level (Table 3).

Acknowledgments. S. Tommasini is thanked for Rb/Sr analysis and comments. We enjoyed the collaboration of D. Bernoulli and H. Stel during part of the sampling. J. Hunziker provided us with interesting unpublished data. A. Mottana kindly made us aware of and sent us relevant articles. Financial support from NFP20 Swiss Science Foundation for some of the samples is acknowledged. This is NSG (Netherlands Research School on Sedimentary Geology) publication 980806.

References

Assereto, R., A. Bosellini, N. Fantini Sestini, and W.C. Sweet, The Permian-Triassic boundary in the Southern Alps, in *The Permian and Triassic Systems and Their Mutual Boundary*, edited by A. Logan and L.V. Hills, *Mem. Can. Soc. Pet. Geol.*, *2*, 176-199, 1973.

Bally, A.W., D. Bernoulli, G.A. Davis, and L. Montadert, Listric normal faults, *Oceanol. Acta*, Sp. Vol. 87-101, 1981.

Bassi, G., Relative importance of strain rate and rheology for the mode of continental extension, *Geophys. J. Int.*, *122*, 195-210, 1995.

Bernoulli, D., Zur Geologie des Monte Generoso (Lombardische Alpen), *Beitr. Geol. Karte Schweiz*, *18*, 1-134, 1964.

Bernoulli, D., C. Caron, P. Homewood, O. Kälin, and J. van Stuijvenberg, Evolution of continental margins in the Alps, *Schweiz. Mineral. Petrogr. Mitt.*, *59*, 165-170, 1979.

Bertotti, G., Early Mesozoic extension and Alpine shortening in the western Southern Alps: The geology of the area between Lugano and Menaggio (Lombardy, Northern Italy), *Mem. Sci. Geol.*, *43*, 17-123, 1991.

Bertotti, G., and M. ter Voorde, Thermal effects of normal faulting during rifted basin formation, 2, The Lugano-Val Grande normal fault and the role of pre-existing thermal anomalies, *Tectonophysics*, *240*, 145-157, 1994.

Bertotti, G., V. Picotti, D. Bernoulli, and A. Castellarin, From rifting to drifting: Tectonic evolution of the South-Alpine upper crust from the Triassic to the Early Cretaceous, *Sediment. Geol.*, *86*, 53-76, 1993a.

Bertotti, G., G.-B. Siletto, and M.I. Spalla, Deformation and metamorphism associated with crustal rifting: The Permian to Liassic evolution of the Lake Lugano-Lake Como area (Southern Alps), *Tectonophysics*, *226*, 271-284, 1993b.

Bertotti, G., M. ter Voorde, S. Cloetingh, and V. Picotti, Thermomechanical evolution of the South-Alpine rifted margin (north Italy): Constraints on the strength of passive continental margins, *Earth Planet. Sci. Lett.*, *146*, 181-193, 1997.

Bill, M., F. Bussy, M. Cosca, H. Masson, and J.C. Hunziker, High-precision U/Pb and $^{40}Ar/^{39}Ar$ dating of an Alpine ophiolite (Gets nappe, French Alps), *Eclogae Geol. Helv.*, *90*, 43-54, 1997.

Brack, P., and H. Rieber, Towards a better definition of the Anisian/Ladinian boundary: New biostratigraphic data and correlations of boundary sections from the Southern Alps, *Eclogae Geol. Helv.*, *86*, 415-527, 1993.

Brusca, C., M. Gaetani, F. Jadoul, and G. Viel, Paleogeografia ladinico-carnica e metallogenesi del sudalpino, *Mem. Soc. Geol. Ital.*, *22*, 65-82, 1981.

Buck, W.R., Modes of continental lithospheric extension, *J. Geophys. Res.*, *96*, 20161-20178, 1991.

Diella, V., M.I. Spalla, and A. Tunesi, Contrasting thermomechanical evolutions in the South Alpine metamorphic basement of the Orobic Alps (Central Alps, Italy), *J. Metamorph. Geol.*, *10*, 203-219, 1992.

El Tahlawi, M.R., Geologie und Petrographie des nordöstlichen Comerseegebietes (Provinz Como, Italien), Ph.D. Thesis, 199 pp., Eidgenossische Technische Hochschule Zurich, Switzerland, 1965.

Ferrara, G., and F. Innocenti, Radiometric age evidence of a Triassic thermal event in the Southern Alps, *Geol. Rundsch.*, *63*, 572-581, 1974.

Foster, D.A., and C.M. Fanning, Geochronology of the northern Idaho batholith and the Bitterrot core complex: Magmatism preceding and contemporaneous with extension, *Geol. Soc. Am. Bull., 109,* 379-394, 1997.

Garzanti, E., The sandstone memory of the evolution of a Triassic volcanic arc in the Southern Alps, Italy, *Sedimentology, 32,* 423-433, 1985.

Gleadow, A.J.W., Fission track dating: What are the real alternatives?, *Nucl. Tracks, 6,* 99-107, 1981

Govers, R., and M.J.R Wortel, Initiation of asymmetric extension in continental lithosphere, *Tectonophysics, 223,* 75-96, 1993.

Green, P.F., A new look at statistics in fission track dating, *Nucl.Tracks, 5,* 121-128, 1981.

Hendrie, D.B., N.J. Kusznir, and R.H. Hunter, Jurassic extension estimates for the North Sea "triple junction" from flexural backstripping: Implications for decompression melting models, *Earth Planet. Sci. Lett., 116,* 113-127, 1993.

Hodges, K.V., and S.A. Bowring, $^{40}Ar/^{39}Ar$ thermochronology of isotopically zoned micas: Insights from the southwestern USA Proterozoic orogen, *Geochim. Cosmochim. Acta, 59,* 3205-3220, 1995.

Hunziker, J.C., J. Desmons, and A.J. Hurford, Thirty-two years of geochronological work in the Central and Western Alps: A review on seven maps, *Mém. Géol. Lausanne, 13,* 1-59, 1992.

Hurford, A.J., and P.F. Green, The zeta age calibration of fission track dating, *Isot. Geosci., 1,* 285-317, 1983.

Kusznir, N.J., and R.G. Park, The extensional strength of the continental lithosphere: Its dependence on geothermal gradient, and crustal composition and thickness, in *Continental Extensional Tectonics,* edited by M.P. Coward, J.F. Dewey, and P.L. Hancock, *Geol. Soc. Spec. Publ., 28,* 35-52, 1987.

Layer, P.W., C.M. Hall, and D. York, The derivation of $^{40}Ar/^{39}Ar$ age spectra of single grains of hornblende and biotite by laser step-heating, *Geophys. Res. Lett., 14,* 757-760, 1987.

Lister, G.S., and S.L. Baldwin, Plutonism and the origin of metamorphic core complexes, *Geology, 21,* 607-610, 1993.

Ludwig, K.R., Isoplot 2.71: A plotting and regression program for radiogenic isotope data, *U.S. Geol. Surv. Open File Rep., 44,* 91-445, 1994.

Lynch, H.D., and P. Morgan, The tensile strength of the lithosphere and the localization of extension, in *Continental Extensional Tectonics,* edited by M.P. Coward, J.F. Dewey, and P.L. Hancock, *Geol. Soc. Spec. Publ., 28,* 53-65, 1987.

Mottana, A., M. Nicoletti, C. Petrucciani, G. Liborio, L. de Capitani, and R. Bocchio, Pre-alpine and alpine evolution of the South-alpine basement of the Orobic Alps, *Geol. Rundsch., 74,* 353-366, 1985.

Nicolas, A., U. Achauer, and M. Daigniers, Rift initiation by lithospheric rupture, *Earth Planet. Sci. Lett., 123,* 281-298, 1994.

Odin, G.-S., Geological time scale, *C.R. Acad. Sci., 318, ser. II,* 59-71, 1994.

Ohnenstetter, M., D. Ohnenstetter, P. Vidal, J. Cornichet, D. Hermuitte, and J. Mace, Crystallization and age of zircon from Corsican ophiolitic albitites: Consequences for oceanic expansion in Jurassic times, *Earth Planet. Sci. Lett., 54,* 397-408, 1981.

Olsen, K.H., and P. Morgan, Introduction: Progress in understanding continental rifts, in *Continental Rifts: Evolution, Structure, Tectonics,* edited by K.H. Olsen, *Dev. Geotecton., 25,* 3-26, 1995.

Phillips, D., and T.C. Onstott, Argon isotopic zoning in mantle phlogopite, *Geology, 16,* 542-546, 1988.

Sanders, C.A.E., G. Bertotti, S. Tommasini, G.R. Davies, and J.R. Wijbrans, Triassic pegmatites in the Mesozoic middle crust of the Southern Alps (Italy): Fluid inclusions, radiometric dating and tectonic implications, *Eclogae Geol. Helv., 89,* 505-525, 1996.

Schmid, S.M., O.A. Pfiffner, G. Schönborn N. Froitzheim, and E. Kissling, Integrated cross section and tectonic evolution of the Alps along the Eastern Traverse, in *Deep Structure of the Alps: Results of NRP 20,* edited by O.A. Pfiffner et al., pp. 289-304, Birkhäuser, Boston, Mass., 1997.

Schumacher, M.E., G. Schönborn, D. Bernoulli, and H.P. Laubscher, Rifting and collision in the Southern Alps, in *Deep Structure of the Alps: Results of NRP 20,* edited by O.A. Pfiffner et al., pp. 186-204, Birkhäuser, Boston, Mass., 1997.

Seward, D., Cenozoic basin histories determined by fission track dating of basement granites, South Island, New Zealand, *Chem. Geol., 79,* 31-48, 1989.

Siletto, G.-B., M.I. Spalla, A. Tunesi, M. Nardo, and L. Soldo, Structural analysis of the Lario basement (Central Southern Alps, Italy), *Mem. Soc. Geol. Ital., 45,* 93-100, 1990.

Spadini, G., S. Cloetingh, and G. Bertotti, Thermo-mechanical modelling of the Tyrrhenian Sea: Lithospheric necking and kinematics of rifting, *Tectonics, 14,* 629-644, 1995.

ter Voorde, M., and G. Bertotti, Thermal effects of normal faulting during rifted basin formation, 2, A finite difference model, *Tectonophysics, 240,* 133-144, 1994.

Vavra, G., D. Gebauer, R. Schmid, and W. Compton, Multiple zircon growth and recrystallization during polyphase Late Carboniferous to Triassic metamorphism in granulites of the Ivrea Zone (Southern Alps): An ion microprobe (SHRIMP) study, *Contrib. Mineral. Petr., 122,* 337-358, 1996.

Veevers, J.J., Middle/Late Triassic (230±5Ma) singularity in the stratigraphic and magmatic history of the Pangean heat anomaly, *Geology, 17,* 784-787, 1989.

von Blanckenburg, F., I.M. Villa, H. Baur, G. Morteani, and R. Steiger, Time calibration of a PT path from the western Tauern window, Eastern Alps; The problem of closure temperatures, *Contrib. Mineral. Petrol., 101,* 1-11, 1989.

Vonderschmitt, L., Bericht uber die Exkursion der Schweizerischen Geologischen Gesellschaft in den Süd Tessin, *Eclogae Geol. Helv., 33,* 205-219, 1940.

Wijbrans, J.R., M. Schliestedt, and D. York, Single grain argon laser probe dating of phengites from the blueschist to greenschist transition on Sifnos (Cyclades, Greece), *Contrib. Mineral. Petrol., 104,* 582-593, 1990.

Wijbrans, J.R., M.S. Pringle, A.A.P. Koppers, and R. Scheveers, Argon geochronology of small samples using the Vulkaan argon laserprobe, *Verh. K. Ned. Acad. Wet., 98,* 181-218, 1995.

Winterer, E.L., and A. Bosellini, Subsidence and sedimentation on Jurassic passive continental margin, Southern Alps, Italy, *AAPG Bull., 65,* 394-421, 1981.

Wright, N., P.W. Layer, and D. York, New insights into thermal history from single grain $^{40}Ar/^{39}Ar$ analysis of biotite, *Earth Planet. Sci. Lett., 104,* 70-79, 1991.

Yamada, R., T. Tagami, S. Nishimura, and I. Hisatoshi, Annealing kinetics of fission track in zircon and experimental study, paper presented at International Workshop on Fission-Track dating, University of Gent, Belgium, 1996.

G. Bertotti, M. ter Voorde, and J. Wijbrans, Faculty of Earth Sciences, Vrije Universiteit, de Boelelaan 1085, 1081 HV Amsterdam, Netherlands. (bert@geo.vu.nl; wijj@geo.vu.nl; voorn@geo.vu.nl)

A.J. Hurford, Department of Geology, University College London, Gower Street, London WC1E 6BT, Great Britain. (T.Hurford@ucl.ac.uk)

D. Seward, Geologisches Institut, Eidgenossische Technische Hochschule Zentrum, 8092 Zurich, Switzerland. (diane@erdw.ethz.ch)

(Received October 17, 1997;
revised October 26, 1998;
accepted October 26, 1998.)